Experimental and Theoretical Study of the Electronic Spectrum of the Methylene Amidogen Radical (H_2CN): Verification of the $^2A_1 \leftarrow {}^2B_2$ Assignment

Alexey Teslja,[†,§] Paul J. Dagdigian,[*,†] Michael Banck,[‡] and Wolfgang Eisfeld[*,‡]

Department of Chemistry, The Johns Hopkins University, Baltimore, Maryland 21218-2685, and Lehrstuhl für Theoretische Chemie, Technische Universität München, Lichtenbergstrasse 4, D-85747 Garching, Germany

Received: March 14, 2006; In Final Form: April 28, 2006

A collaborative experimental and theoretical study of the electronic spectrum and excited-state photochemistry of H_2CN has been carried out. The absorption spectrum, in the range of 287−278 nm, was measured through cavity ring-down spectroscopy. The radical was prepared by 193 nm photolysis of monomeric formaldoxime vapor. Two diffuse features were observed in the 34800−35800 cm^{-1} spectral range, along with the A−X (1,0) band of the OH cofragment. The broad features were assigned through high-level ab initio calculations as vibronic transitions to the ground and $2b_1$ (umbrella mode) levels of the second excited $\tilde{B}\ ^2A_1$ state from the ground $\tilde{X}\ ^2B_2$ state of H_2CN. Rotational constants for the lower and upper levels of these transitions were computed from the expectation values of the moments of inertia tensor, using the appropriate vibrational wave functions. Experimental and simulated rotational profiles of these bands agree extremely well with each other for an assumed type-B electric dipole-allowed $^2A_1 \leftarrow {}^2B_2$ transition appropriate to this transition. The former assignment to the dipole-forbidden $^2B_1 \leftarrow {}^2B_2$ transition can be ruled out by these results. A theoretical investigation of the dissociation pathways for electronically excited H_2CN is also presented. The upper states of the observed bands cannot dissociate directly but rather decay through internal conversion and subsequent dissociation to H + HCN fragments; higher b_1 levels are above the excited-state dissociation limit.

1. Introduction

The methylene amidogen radical (H_2CN) has been the subject of a number of experimental and theoretical studies both because of its importance as an intermediate in certain chemical processes and its apparently complicated photophysics.[1] In particular, this radical plays a role in the decomposition of nitramine propellants and in the chemistry of extraterrestrial atmospheres.

Despite a number of studies over almost 40 years, there still remain significant questions about the electronic spectrum of H_2CN. Several diffuse bands of H_2CN at transition wavenumbers around 35 000 cm^{-1} were first observed in flash photolysis experiments using both formaldoxime (H_2CNOH) and formaldazine ($H_2CN-NCH_2$) as precursors.[2−4] Jacox[5] also observed similar features at slightly lower excitation energies in absorption spectra of H_2CN trapped in cryogenic argon matrices. Dagdigian et al.[6] tried but failed to detect these bands in a gas-phase laser fluorescence excitation spectroscopy study, although signals due to the OH fragment from photolysis of the formaldoxime precursor were observed. In a molecular beam experiment employing pyrolysis of formaldazine to generate H_2CN, Davis and co-workers[7] observed the H_2CN electronic absorption bands through action spectroscopy, in which H atom fragments were detected by Rydberg atom time-of-flight (TOF) spectroscopy. More recently, Nizamov and Dagdigian[8] employed cavity ring-down spectroscopy (CRDS) to record high-quality room-temperature absorption spectra of H_2CN generated in a cell by photolysis of formaldoxime. Vibrational transitions in the infrared spectral region for H_2CN embedded in a cryogenic argon matrix have been reported by Jacox.[5] The microwave spectrum of H_2CN has also been recorded, and precise rotational constants have been published.[9]

Complementary to these experimental studies have been a number of theoretical investigations of the electronic states of H_2CN.[10−18] These studies have guided the interpretations of the more recent experiments. The ground electronic state of H_2CN is well established as having $^2B_2$ symmetry.[1] Adams et al.[11] calculated that the first vertically excited state has $^2B_1$ symmetry. So[10] found that the lowest adiabatically excited state has a nonplanar equilibrium geometry, with $^2A'$ symmetry. Brinkmann et al.[15] predicted that the lowest excited state to be of $^2B_1$ symmetry, with two higher excited states: a second $^2B_1$ and a $^2A_1$ state. The lowest $^2A_1$ state was calculated to be planar, whereas the second $^2B_1$ state was predicted to relax to a nonplanar equilibrium structure. The investigators in the recent experimental studies have looked upon the first $^2B_1$ state as the most likely upper state of the observed electronic transition.[7,8]

A $^2B_1 \leftarrow {}^2B_2$ transition in H_2CN is electronically forbidden but can be allowed vibronically. In their photofragment spectroscopy experiment, Davis and co-workers[7] reported a slightly negative recoil anisotropy parameter ($\beta = -0.10 \pm 0.03$) for the H atom fragments. This was interpreted in a model of direct dissociation[19] as being consistent with a vibronically allowed $^2B_1 \leftarrow {}^2B_2$ transition, but inconsistent with an electric dipole-allowed $^2A_1 \leftarrow {}^2B_2$ transition. It is well known that the rotational structure of a polyatomic band can be analyzed to determine the inertial axis along which the transition moment lies,[20] and

* To whom correspondence should be addressed. P.J.D.: E-mail, pjdagdigian@jhu.edu; fax, 1-410-516-8420. W.E.: E-mail, wolfgang.eisfeld@ch.tum.de; fax, 49-89-289 13 622.

† The Johns Hopkins University.

§ Present address: Department of Chemistry, Columbia University, New York, NY 10027.

‡ Technische Universität München.

10.1021/jp061578j CCC: $33.50
Published on Web 06/02/2006

hence the symmetry relation between the upper and lower electronic states. Nizamov and Dagdigian[8] compared their measured rotational contours with a simulation based on a vibronically allowed $^2B_1 \leftarrow {}^2B_2$ (C-type) transition. Detailed comparison of the experimental and simulated band contours was not entirely satisfactory.

A recent theoretical investigation of the electronic states of H_2CN by Eisfeld[16] has shed new light on this problem. These high-level ab initio calculations predict lower excitation energies than in previous theoretical studies. Eisfeld assigned the observed electronic transition as the dipole-allowed $\tilde{B}\ ^2A_1 \leftarrow \tilde{X}\ ^2B_2$ transition, involving the second excited state ($\tilde{B}\ ^2A_1$). The intensities of both dipole-allowed and dipole-forbidden but vibronically-allowed bands were computed. The two bands observed in the spectrum of H_2CN were assigned as the origin band and the 4_0^2 band, where the latter involves excitation of two quanta of the ν_4 (b_1) umbrella mode in the excited electronic state.

In further work, Eisfeld[17] carried out a theoretical study of the photodetachment spectrum of the H_2CN radical. The electron affinity of H_2CN was computed very accurately, and electron detachment energies were calculated by complete active-space and multiconfiguration self-consistent field (CASSCF and MCSCF), as well as multireference configuration interaction (MRCI) methods. The MRCI wave functions were employed to compute electron detachment energies. Detachment to the excited neutral $\tilde{A}\ ^2B_1$ and $\tilde{B}\ ^2A_1$ states were shown to be clearly distinguishable. The photodetachment of a H_2CN^- anion has been investigated experimentally, but at a photon energy sufficient to access only the ground $\tilde{X}^2\ B_2$ electronic state of neutral H_2CN.[21]

In this paper, we present cavity ring-down (CRD) absorption spectra of H_2CN taken at lower concentrations than recorded by Nizamov and Dagdigian.[8] We also make a detailed comparison of the experimental spectra with rotational contours computed with rotational constants obtained by averaging over the b_1 umbrella motion on the ground and excited-state potential energy surfaces.[16] The experimental and simulated spectra agree extremely well with each other for an assumed type-B transition, appropriate to a $^2A_1 \leftarrow {}^2B_2$ transition, and disagree significantly if the transition moment is assumed to lie along the *a* or *c* inertial axes. This provides strong confirmation for the $^2A_1 \leftarrow {}^2B_2$ assignment made previously by Eisfeld.[16] We also offer possible explanations for the value of the β parameter measured by Davis and co-workers,[7] which is seemingly inconsistent with this assignment. The theoretical investigation of the dissociation pathways for electronically excited H_2CN is also presented. We also summarize details of the electronic spectrum of H_2CN which have yet to be explained.

2. Experimental Section

New measurements of the CRD absorption spectrum of methylene amidogen were made in a recently constructed apparatus, schematically illustrated in Figure 1, suitable for studies at elevated temperatures. The central portion of the cell is 3.5 cm in diameter and 41 cm long, and a 10 cm long section in the center could be heated. The CRD mirrors (Research Electro Optics, Boulder, CO, 99.8% reflectivity at ~280 nm, estimated from the photon decay lifetimes) were mounted 105 cm apart. With these mirrors, the empty-cavity decay lifetime was approximately 1 order of magnitude longer than in our previous experimental study,[8] which leads to a corresponding increase in the detection sensitivity. The photolysis and probe laser beams cross at an angle of 2.9° in the center of the cell.

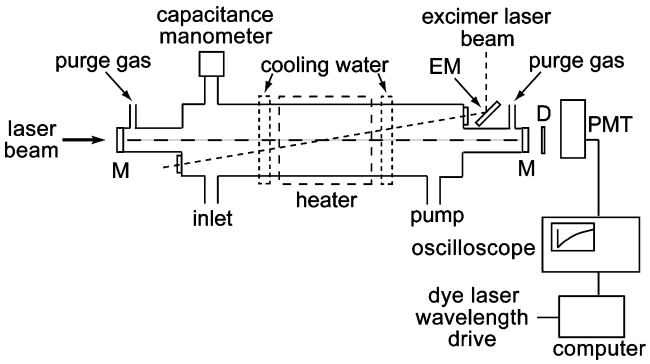

Figure 1. Schematic diagram of the cavity ring-down apparatus (not to scale). M denotes high-reflectivity mirrors for ~285 nm; EM, mirror for 193 nm; D, diffuser; and PMT, photomultiplier tube.

The diameter of the excimer beam entering the cell was determined by an iris (1 cm d.) at the entrance to the cell, and the beam was focused in the direction perpendicular to the plane of the laser beams with a cylindrical cell (1 m focal length). The length over which the photolysis laser beam overlaps the probe laser beam is ~10 cm.

Methylene amidogen and the cofragment OH were generated by 193 nm photolysis of formaldoxime. Formaldoxime polymer was synthesized as described previously.[8,22] To generate flows of monomeric formaldoxime diluted in a buffer gas (He or Ar), the buffer gas was flowed through a glass tube filled with the solid polymer and heated to ~50 °C. The polymer was packed between plugs of glass wool to prevent formaldoxime dust from entering the chamber. A small flow of buffer gas was directed at the mirrors to minimize reduction in their reflectivity.

The frequency-doubled output from a tripled Nd:YAG (Continuum Surelite I) pumped dye laser (Lambda Physik FL3002E) was injected into the optical cavity through one of the high-reflectivity mirrors. The second harmonic was separated from the fundamental dye laser radiation by a set of four Pellin-Broca prisms. The temporal width of a laser pulse was ~5 ns, and the spectral bandwidth of the doubled UV output was 0.4 cm^{-1}. The typical UV pulse energy was 0.5 mJ. An aperture was employed to control the size of the UV beam in order to reduce the number of transverse modes excited in the cavity. The CRD signal was detected through the rear mirror with a Hamamatsu R282 photomultiplier tube (PMT). A diffuser was placed in front of the PMT to minimize possible problems arising from the nonuniformity of the PMT area response. The photolysis light source was a Lambda Physik COMPex 102 excimer laser. The typical pulse energy of the excimer laser beam entering the vacuum chamber was 10 mJ. The delay between the excimer and probe lasers was controlled by a digital delay generator controlled by the data acquisition computer.

The CRD signal from the PMT was detected with a LeCroy LT372 digital oscilloscope. The signal from each shot was transferred through a GPIB connection to the computer, and a weighted linear least-squares fit of the logarithm of the signal as a function of time was employed to compute the photon decay lifetime from each laser shot. At a given wavelength, single-shot decay lifetimes were averaged over a preset number of shots (10−30) with the excimer laser on and off on alternate shots, and then the dye laser wavelength was stepped to the next wavelength. The signal due to the photolysis products was computed by subtracting the decay constant with the excimer laser off from that with the excimer laser on. Ring-down lifetimes could be determined to an accuracy of 1.5% in a 10-shot average.

3. Computational Details

The electronic structure calculations were performed using high-level ab initio methods to account for dynamic electron correlation. For the ground-state calculations the spin-restricted coupled-cluster singles doubles method with pertubative triples [RCCSD(T)] was used. The calculations of excited states and the dissociation pathways require multireference treatments to describe the static correlation correctly. First, a multiconfiguration self-consistent field (MCSCF) calculation is performed to optimize the one-electron basis of the reference states, averaging over all states included in the respective calculation. As active space, 12 occupied orbitals (8 a_1, 2 b_2 and 2 b_1) for methylene amidogen and 11 occupied orbitals (7 a_1, 2 b_2 and 2 b_1) for hydrogen cyanide were selected. The two lowest a_1 orbitals were considered closed, resulting in a total active space of 10 and 9 orbitals, respectively. Reference configurations were selected according to their weights in the state vectors of complete active-space self-consistent field (CASSCF) calculations along the dissociation pathway and the fragment equilibrium geometries. All configurations with CI coefficients larger than 0.02 were chosen as reference configurations. The selected configurations and the corresponding MCSCF reference wave functions are then used to perform internally contracted multireference configuration interaction (MRCI) calculations of the state energies.[23,24] The MRCI energies are corrected by the multireference version of the Davidson correction.[25] All calculations were performed using the augmented correlation consistent basis sets of Dunning et al.[26,27] as atomic orbital basis which are denoted by AVTZ, AVQZ, and AV5Z. The ab initio calculations were carried out by the MOLPRO suite of programs.[28]

Geometry optimizations were performed in symmetry coordinates by an external optimization program based on the partitioned rational function method. Gradients were computed numerically by finite differences. For the obtained equilibrium geometries, the second derivative and respective force constant matrices were calculated, also employing symmetry coordinates and finite differences. These force constant matrices were then transformed into mass-weighted Cartesian force constant matrices from which vibrational frequencies and normal modes were obtained by diagonalization.

4. Results

4.1. Electronic Spectrum and Band Contour Analysis. Figure 2 presents a CRD absorption spectrum of photolyzed formaldoxime, with sufficient time between photolysis and detection to allow for thermalization of the photolysis products (argon buffer gas at 2.6 Torr and a delay of 100 μs). Transitions in both photolytic fragments, H_2CN and OH, are visible in the spectrum. As in the early flash photolysis study of Ogilvie and Horne[2] and our previous CRDS study,[8] two broad features due to H_2CN, as well as the sharp rotational lines of the A−X (1,0) band of OH, are observed in the spectrum. The OH lines were used for wavelength calibration. The spectral region that could be scanned was limited by the wavelength range for which the CRD mirrors had high reflectivity.

A detailed comparison of the present and our previous CRD spectra revealed some differences. Figure 3 compares electronic spectra of H_2CN recorded in the flash photolysis study by Ogilvie and Horne,[2] our two CRDS studies, and the H atom photofragment study by Davis and co-workers.[7] The transition wavenumber and profile of the shorter-wavelength band (at 281 nm) in the two CRD spectra agree well, whereas there is a noticeable difference in the peak position and shape of the longer-wavelength band (at 285 nm) in the two spectra. We believe that the photolysis-probe delay was sufficiently long in both of our CRDS studies that the H_2CN was collisionally relaxed. We have carried out simulations of the bands (discussed in detail below) at room and elevated temperatures and find that the fwhm of both bands increase similarly with temperature.

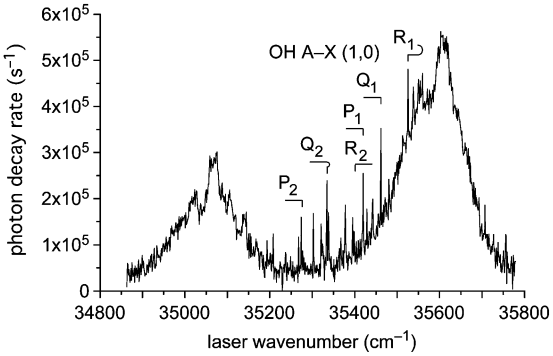

Figure 2. Cavity ring-down absorption spectrum of photolyzed formaldoxime (estimated partial pressure ~0.05 Torr in 2.6 Torr argon). The spectrum was recorded with a delay of 100 μs between the photolysis and probe laser pulses. Under these conditions, the H_2CN and OH photolytic fragments are thermally equilibrated. The apparatus was at room temperature. The broad features are vibronic transitions of H_2CN, while the sharp features are rotational lines of the OH A−X (1,0) band. The various rotational branches of the OH band are indicated. The ordinate is the contribution to the CRD photon decay rate from the molecular absorbers, or $\tau^{-1} - \tau_0^{-1}$, where τ and τ_0 are the photon decay lifetimes with the photolysis laser on and off, respectively.

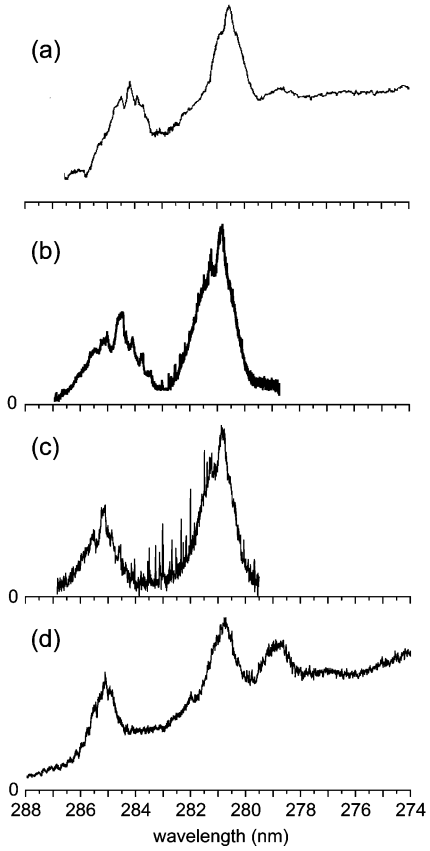

Figure 3. Comparison of electronic spectra, plotted as a function of wavelength, of H_2CN recorded in (a) the flash photolysis study of Ogilvie and Horne (ref 2), (b) previous (ref 8) and (c) our present CRD spectra, and (d) the H atom photofragment study by Davis and coworkers (ref 7). The zero signal level is indicated for panels b−d.

We note that the widths of the 281 nm bands in our CRD spectra (Figure 3, parts b and c) differ only slightly.

We see that the two bands observed in the present CRDS study match fairly well the two longer-wavelength bands which were observed by Davis and co-workers[7] in their H atom photofragment action spectrum. The action spectrum acquired by Davis and co-workers pertains to isolated H_2CN radicals in a molecular beam. The rotational excitation of the radicals is not known, as the radicals were prepared by pyrolysis at ~1000 °C and some cooling occurred in the supersonic expansion into vacuum. It is likely that their rotational temperature is near room temperature, and the band contour in the action spectrum and in a room-temperature absorption spectrum should be similar. We see in Figure 3 that the two bands appearing in our present CRD spectrum match well the overall shape and wavelengths of the corresponding bands in the H atom photofragment action spectrum recorded by Davis and co-workers.[7] Thus, we may assign the molecular carrier of the presently observed bands to isolated H_2CN radicals.

The features assigned to H_2CN in the H atom spectrum of Davis and co-workers[7] appear on a background which increases with decreasing wavelength. This background must be due to photodissociation of residual formaldazine in the molecular beam[29] since this compound does absorb in this wavelength range.[2]

Davis and co-workers[7] also observe a third feature at 279 nm. This feature does not appear to be present in the room-temperature CRD spectrum. Since vibrational excitation in H_2CN produced by pyrolysis would not be expected to be cooled efficiently in the free-jet expansion, it seems reasonable to assign this as a hot band transition. The lowest-energy vibrational frequencies in the $\tilde{X}\ ^2B_2$ states are reported[5] as 913 (ν_6, b_2, CH_2 rocking) and 954 (ν_4, b_1, umbrella) cm^{-1}. The calculations of Eisfeld[16] suggest that the strongest vibronic transitions out of these levels would be excitation to the corresponding fundamental vibrational levels in the $\tilde{B}\ ^2A_1$ excited state. Since the vibrational frequencies in the $\tilde{B}\ ^2A_1$ state are computed[16] to be significantly smaller than in the ground state, these hot band transitions are predicted to lie to the red of the origin band. Hence, the assignment of the feature at 279 nm as a hot band seems unlikely. We are unable to make a convincing assignment for this feature to a vibronic transition in H_2CN.

We see in Figure 3 that the 285 nm band in the flash photolysis absorption spectrum[2] is shifted slightly in wavelength from the corresponding band in both the H atom photofragment action spectrum and our present CRD spectrum. In fact, this band bears a strong resemblance to the corresponding band in our previous[8] CRD spectrum. The CRD detection sensitivity in that study was approximately an order of magnitude less than that of the present study, because of a lower mirror reflectivity; from the observed[8] absorption per pass, the concentration was an order of magnitude higher than in the present study. The concentration in the flash photolysis experiment[2] was also significantly higher than in the present study. It appears that the molecular concentration affects that profile of the 285 nm band. We were not able in the present study to vary the experimental conditions sufficiently to observe an evolution of the spectrum displayed in Figure 2 into that reported[8] previously. We do not offer a physical explanation for the observed spectral changes in the 285 nm band but instead proceed with a comparison of the presently observed CRD absorption spectrum with spectral simulations based on a computational treatment of the H_2CN electronic states.

TABLE 1: Computed H_2CN Rotational Constants

	rotational constant (cm^{-1})		
level[a]	*A*	*B*	*C*
	$\tilde{X}\ ^2A_1$ State		
equil geom[b]	9.5213	1.2962	1.1409
ground[c]	9.4401	1.2943	1.1406
expt[d]	9.4844	1.3062	1.1423
	$\tilde{B}\ ^2B_2$ State		
equil geom[b]	9.2422	1.2633	1.1114
ground[c]	8.9938	1.2570	1.1102
$2\nu_4$	8.0985	1.2318	1.1053

[a] The number before b_1 denotes the number of quanta in the ν_4 (b_1) umbrella mode. [b] Rotational constants computed from the MRCI equilibrium geometry (equil geom) (AVQZ basis), from Table 1 of ref 16. [c] Ground vibrational level. [d] Reference 9.

It is well known that the orientation of the transition dipole with respect to the molecular framework can be determined from the rotational structure of a band.[20] The transition dipole for the $\tilde{B}\ ^2A_1 \leftarrow \tilde{X}\ ^2B_2$ transition lies in the molecular plane perpendicular to the C−N bond and hence lies along the *b* inertial axis of the molecule. To provide experimental confirmation of this assignment[16] for the observed electronic transition in H_2CN, we compare our experimental scans of the observed H_2CN bands with simulations of a type-B transition (transition moment along the *b* inertial axis), using rotational constants obtained from our ab initio study of H_2CN electronic states.[16]

Table 1 presents rotational constants computed from the equilibrium geometries[16] of the $\tilde{X}\ ^2B_2$ and $\tilde{B}\ ^2A_1$ states. In addition, rotational constants were computed by an appropriate average over the ν_4 (b_1) umbrella vibrational coordinate, since the 281 nm band has been assigned[16] as involving excitation of two quanta of the ν_4 mode. In this vibrational averaging, the rotational constants were computed from one-dimensional expectation values of the moment of inertia tensor over the vibrational wave functions of the ν_4 mode for various vibrational levels of the upper or lower electronic state. It can be seen in Table 1 that for the $\tilde{X}\ ^2B_2$ ground vibronic level there are only small differences in the rotational constants, mainly in the *A* rotational constant, computed from the equilibrium geometry and by averaging over the ν_4 vibrational coordinate.

Also included in Table 1 are the rotational constants of the ground vibronic level determined by microwave spectroscopy.[9] It can be seen that the computed rotational constants for the ground vibronic level are in good agreement with these experimental values. This suggests that our theoretical treatment has provided a very reliable determination of the equilibrium geometry of the ground $\tilde{X}\ ^2B_2$ state.

In contrast to the situation of the ground electronic state, in the $\tilde{B}\ ^2A_1$ excited state there are much larger differences in the rotational constants, again principally in the *A* rotational constant, computed from the equilibrium geometry and by averaging over the ν_4 vibrational coordinate for the ground and $2\nu_4$ vibrational levels. In fact, the *A* rotational constant is computed to decrease significantly with excitation of the ν_4 mode in the $\tilde{B}\ ^2A_1$ excited state. These larger differences for the $\tilde{B}\ ^2A_1$ state reflect the fact that the ν_4 umbrella mode is much more floppy in the excited state than in the ground electronic state.[16] Rotational constants were also computed from one-dimensional averages over all the other vibrational coordinates; in all cases the rotational constants differed only slightly from the values obtained for the equilibrium geometries. Hence, it is reasonable to consider averaging over the ν_4 umbrella mode only for the purpose of computing rotational constants to be

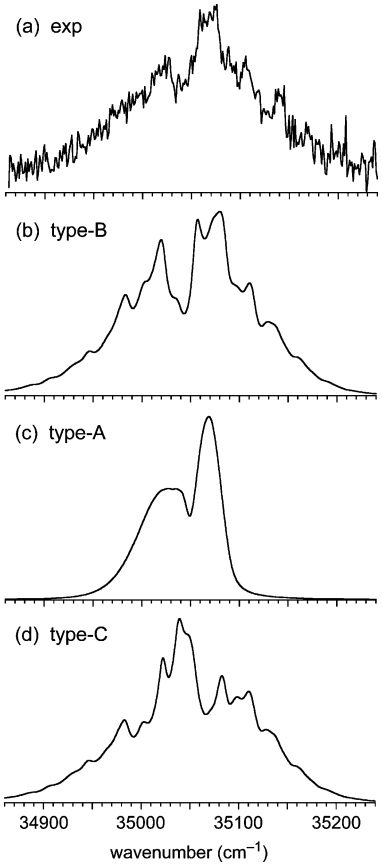

Figure 4. Comparison of (a) the experimental CRD spectrum of the 285 nm band, assigned as the origin band of the $\tilde{B}\ ^2A_1 \leftarrow \tilde{X}\ ^2B_2$ transition, with room-temperature simulations using the rotational constants given in Table 1, with the electronic transition moment assumed to lie on (b) the *b*, (c) the *a*, and (d) the *c* inertial axes. In the simulations, a room-temperature rotational distribution was assumed, and nuclear spin statistics were taken into account. Each rotational line was taken to have a Lorentzian profile, with Γ equal to 12 cm^{-1}.

used in spectral simulations, especially with the significant lifetime (Lorentzian) broadening in the spectrum (see below).

If the line widths were determined by the laser line width, or from the purely radiative lifetime, then the electronic spectrum of H_2CN would show rotationally resolved lines, as in the spectrum of formaldehyde,[20] which has rotational constants similar in magnitude to those of H_2CN. However, from the observation of H atom fragments upon electronic excitation,[7] the $\tilde{B}\ ^2A_1$ excited state is known to decay nonradiatively, and the excited-state dissociation leads to a significant Lorentzian broadening. As can be seen in Figure 2, the electronic spectrum of H_2CN is thus not rotationally resolved. We therefore compare the experimental spectrum with spectra simulated using the rotational constants given in Table 1. We have taken a rigid-rotor Hamiltonian for both the upper and lower vibronic levels. In these simulations, we take account of the nuclear spin statistics and weight the rotational levels as follows: *ee* and *eo*, 3; *oo* and *oe*, 1. We take Lorentzian line profiles, with widths (parametrized by Γ, the fwhm of the line) adjusted to fit the experimental spectra. The rotational temperature was taken as 298 K, since the H_2CN radicals are rotationally equilibrated during the delay between the photolysis and CRD probe laser pulses.

Figure 4 presents comparisons of the experimentally recorded spectrum (panel a) of the origin band, at 285 nm, with simulations assuming that the transition moment lies along one of

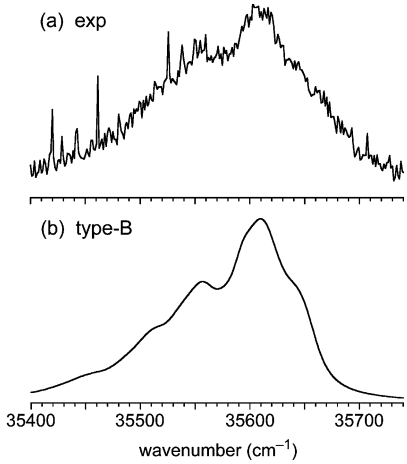

Figure 5. Comparison of (a) the experimental CRD spectrum of the 281 nm band, assigned as the 4_0^2 band of the $\tilde{B}\ ^2A_1 \leftarrow \tilde{X}\ ^2B_2$ transition, with (b) a room-temperature simulation using the rotational constants given in Table 1, with the electronic transition moment assumed to lie on the *b* inertial axis. In the simulation, a room-temperature rotational distribution was assumed, and nuclear spin statistics were taken into account. Each rotational line was taken to have a Lorentzian profile, with Γ equal to 25 cm^{-1}.

the inertial axes. It can be seen that the assumption of a type-B transition provides a very good representation of the experimental spectrum. By contrast, simulations assuming a type-A or -C transition (Figure 4, parts c and d) do not reproduce the experimental spectrum very well at all. This provides strong experimental confirmation for the $\tilde{B}\ ^2A_1 \leftarrow \tilde{X}\ ^2B_2$ assignment of the observed transition in H_2CN. Simulations of a type-B transition were carried out with various assumed values for the Lorentzian width parameter Γ. A value $\Gamma = 12$ cm^{-1} (with an estimated uncertainty of ± 2 cm^{-1}) was found to provide the best representation of the experimental spectrum. We see in Figure 4b that, while there is extensive overlapping of the broadened lines, the band still shows some rotational structure.

Eisfeld[16] assigned the feature at 281 nm as the 4_0^2 band of the $\tilde{B}\ ^2A_1 \leftarrow \tilde{X}\ ^2B_2$ transition. Figure 5 presents a comparison of the experimental spectrum with a spectrum simulated assuming a type-B transition and using the rotational constants computed for the ground vibronic level and the $2\nu_4$ vibrational level of the $\tilde{B}\ ^2A_1$ excited state (see Table 1). We see that the simulated spectrum provides a very good representation of the experimental spectrum, although the width of the experimental band is somewhat broader in the simulated band. In this case, a somewhat larger Lorentzian width ($\Gamma = 25$ cm^{-1}, with an estimated uncertainty of ± 5 cm^{-1}) was required for the simulated spectrum of this band than for representing the origin band. The principal reasons why the 281 nm band has a somewhat different profile than the 285 nm band are the strong excited-state vibrational dependence of the *A* rotational constant and the larger Lorentzian broadening.

Comparison of the experimental and simulated spectra also allow accurate determination of the origins of the observed bands. We derive the band origin transition wavenumbers to be 35 047 and 35 587 cm^{-1} for the 0_0^0 origin and 4_0^2 bands, respectively. As noted previously, the transition wavenumber of the origin band agrees very well with the value (34 646 cm^{-1}) computed by Eisfeld.[16] The difference in the transition wavenumbers of the 0_0^0 and 4_0^2 bands implies that the vibrational energy of the $2\nu_4$ level within the $\tilde{B}\ ^2A_1$ state is 540 cm^{-1}. This is in good agreement with the corresponding value (477 cm^{-1}) computed by Eisfeld.[16]

TABLE 2: RCCSD(T) Optimized Geometries (Bond Lengths in Å, Angles in deg) and Corresponding Relative and Zero-Point Energies (in eV) for Different Reaction Channels

system	basis	*R*C−N	*R*C−H	∠H−C−H	relative energy	ZPE
$H_2CN(\tilde{X}^2B_2)$[a]	AVTZ	1.2496	1.0948	117.8	0.0	0.6761
$H_2CN(\tilde{X}^2B_2)$[a]	AVQZ				0.0	
$H_2CN(\tilde{X}^2B_2)$[a]	AV5Z				0.0	
$HCN(\tilde{X}^1\Sigma^+) + H(^2S)$	AVTZ	1.1601	1.0670	180.0	1.3267	0.4324
$HCN(\tilde{X}^1\Sigma^+) + H(^2S)$	AVQZ				1.3156	
$HCN(\tilde{X}^1\Sigma^+) + H(^2S)$	AV5Z				1.3142	
$HCN(\tilde{a}^3A') + H(^2S)$	AVTZ	1.2973	1.1036	121.1	6.1060	0.3422
$HCN(\tilde{a}^3A') + H(^2S)$	AVQZ				6.1507	
$HCN(\tilde{a}^3A') + H(^2S)$	AV5Z				6.1632	
$CN(X^2\Sigma^+) + 2H(^2S)$	AVTZ	1.1786			7.0290	0.1268
$CN(X^2\Sigma^+) + 2H(^2S)$	AVQZ				7.0536	
$CN(X^2\Sigma^+) + 2H(^2S)$	AV5Z				7.0585	
$CN(X^2\Sigma^+) + H_2(\tilde{X}^1\Sigma_g^+)$	AVTZ	1.1786			2.3217	0.3996
$CN(X^2\Sigma^+) + H_2(\tilde{X}^1\Sigma_g^+)$	AVQZ				2.3197	
$CN(X^2\Sigma^+) + H_2(\tilde{X}^1\Sigma_g^+)$	AV5Z				2.3171	

[a] Reference 16.

Despite the very good agreement of the experimental spectrum and simulations of the rotational contours based on high-level ab initio calculations, there remains one point of significant disagreement between experiment and theory. We see in Figure 2 that the 4_0^2 band is approximately twice as intense as the origin band. By contrast, the intensity of the 4_0^2 band is predicted[16] theoretically to be only 18% of the intensity of the origin band. As suggested by the magnitude of the determined Lorentzian widths and discussed further below, the excited levels have very short lifetimes. This can lead to large changes in computed intensities since short lifetimes are usually induced by strong vibronic coupling effects, which were not taken into account in the previous study.[16]

4.2. Excited-State Dissociation Pathways. Photodissociation after excitation into the $\tilde{B}\ ^2A_1$ state clearly plays a significant role since the H atom photofragment action spectrum has been measured[7] to be in good agreement with the present CRD spectrum. Excited-state dissociation is also one possible explanation for the lack of a vibrational progression above 36 000 cm^{-1} and for the broadening of the rotational lines apparent in the simulations presented in Figures 4 and 5. In principle, the dissociation can take place either on the excited state or, after internal conversion, on the ground state. In any case, three different reaction channels have to be considered of which, however, only channels 1 and 2 yield H atoms:

$$H_2CN \rightarrow HCN + H \quad (1)$$

$$H_2CN \rightarrow CN + 2H \quad (2)$$

$$H_2CN \rightarrow CN + H_2 \quad (3)$$

Channels 1 and 2 are simple bond rupture reactions while in channel 3 the formation of a H−H bond occurs during fragmentation. In the following, these dissociation pathways on the excited-state surfaces are investigated in detail.

4.2.1. Dissociation Energetics. Table 2 lists the optimized geometries and energies of methylene amidogen and the reaction fragments at the RCCSD(T) level of theory for several basis sets. All reactions are endothermic from the ground electronic state. For channel 1, the energy of the reaction leading to hydrogen cyanide in its singlet ground state is only 1.0 eV (taking ZPE into account). The energy of the same channel but with HCN in the triplet state is 4.8 eV higher. A significantly higher reaction energy of 6.5 eV is computed for channel 2 since in this case two C−H bonds are broken simultaneously. By contrast, in channel 3 a H−H bond is formed while two C−H bonds are broken, resulting in a reaction energy of 2.0 eV, which is much lower than that for channel 2. The photon energies corresponding to the observed 285 and 281 nm absorptions are 4.35 and 4.41 eV, respectively. Therefore, only channels 1 and 3 are energetically allowed. The available excess energy after excitation to the $\tilde{B}\ ^2A_1$ state is not sufficient to lead to the triplet state of HCN or to the three-body fragmentation (channel 2).

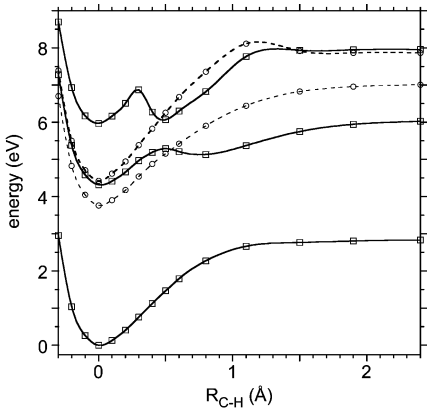

Figure 6. Minimum energy path of $H_2CN \rightarrow HCN + H$ along the H−H bond. Solid lines are $^2A_1$ and $^2B_2$ states, dashed lines are $^2B_1$ states. The relative energy is given in eV, and the reaction coordinate is given in Å.

To obtain a comprehensive picture of the dissociation, it is nevertheless important to look at reaction paths and barriers as well, to determine which H_2CN states at equilibrium geometry are connected to which states at the respective asymptotes and how high possible reaction barriers are. To this end, we have calculated minimum energy paths and linear reaction paths for the three reactions including the five lowest-lying electronic states.

4.2.2. $H_2CN \rightarrow HCN + H$. Figure 6 displays the minimum energy path of the $\tilde{B}\ ^2A_1$ state for hydrogen displacement along a C−H bond axis, corresponding to reaction 1. The geometries were optimized at the CASSCF level of theory at fixed C−H bond lengths, followed by MRCI single point calculations. Because of the asymmetric removal of one hydrogen, the symmetry of the system is lowered from C_{2v} to C_s. At the asymptote, the ground $H_2CN\ \tilde{X}\ ^2B_2$ state is connected to the

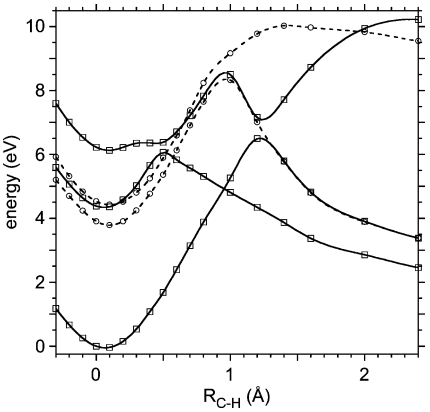

Figure 7. Linear reaction path of $H_2CN \rightarrow CN + H_2$ along the fragment distance. Solid lines are $^2A_1$ and $^2B_2$ states, and dashed lines are $^2B_1$ states. The relative energy is given in eV, and the reaction coordinate is given in Å.

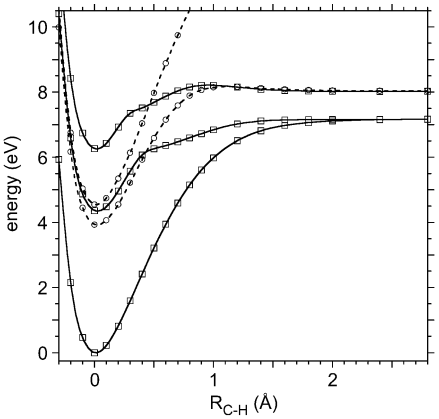

Figure 8. Linear reaction path of $H_2CN \rightarrow CN + 2H$ along the C−H distance. Solid lines are $^2A_1$ and $^2B_2$ states, and dashed lines are $^2B_1$ states. The relative energy is given in eV, and the reaction coordinate is given in Å.

ground, singlet state of HCN, and the bright excited ($\tilde{B}\ ^2A_1$) state is connected to the lowest excited HCN triplet state without a crossing between both. Thus, after electronic excitation, the system is confined to end up in the triplet state of HCN unless internal conversion takes place. The ground state resembles mostly a smooth Morse potential of 2.8 eV well depth. This significantly higher lying asymptote compared to the relative energy of the HCN($\tilde{X}\ ^1\Sigma^+$) + H(^{2}S) given in Table 2 (1.3 eV) is due to the only slightly relaxed (123°) H−C−N angle, whereas the HCN ground state is linear. Both excited A″ states (corresponding to $^2B_1$) follow Morse potentials as well, but are less tightly bound. The excited A′ states (corresponding to $^2A_1$ and $^2B_2$), however, interact strongly with each other, and an avoided crossing can be observed around a C−H displacement of 0.5 Å. This leads to a transition state in the first excited A′ state approximately 1.0 eV above the equilibrium energy. Following the reaction coordinate further, a shallow second minimum is reached at a displacement of around 0.75 Å, which is connected to the global minimum of that potential energy surface via the transition state. This metastable state is located approximately 0.8 eV above the excited-state minimum and 0.16 eV below the transition state. The overall well depth of the second A′ state is around 1.63 eV with respect to the HCN-($\tilde{a}^3A'$) + H(^{2}S) exit channel. As is obvious from Table 2, this channel is thermodynamically inaccessible on the excited-state surface because the available photon energy is below the energy of the asymptote. However, if internal conversion to the ground state occurs, dissociation to HCN($\tilde{X}\ ^1\Sigma^+$) + H(^{2}S) can take place along this path.

4.2.3. $H_2CN \rightarrow CN + H_2$. Figure 7 shows the dissociation/recombination to molecular hydrogen and a cyanide radical (reaction 3) at the MRCI level of theory. The hydrogen distance is decreased to the H_2 equilibrium bond length while the interfragment distance (distance from the center of mass of the hydrogens to the carbon atom) is linearly increased and plotted as a reaction coordinate. The system symmetry is kept at $C2v$ throughout the reaction, keeping the fragment angle fixed at 90°. The ground state has a very high barrier and an avoided crossing with the $^2B_2$ state at a fragment distance of around 1.25 Å. At the asymptote, it becomes degenerate with the first $^2B_1$ state to form the lowest-lying quartet CN state. The bright excited state has a transition state induced by another avoided crossing with a higher lying $^2A_1$ state around 3.25 eV above the equilibrium energy. Upon further increase of the interfragment distance, the energy drops considerably and corresponds to the lowest lying CN(X $^2\Sigma^+$) state, around 0.54 eV below the $^4\Sigma^+$ state and 1.95 eV below the equilibrium energy of the H_2CN $\tilde{B}\ ^2A_1$ state. These results show that a photodissociation leading to CN and H_2 is very unlikely. On the ground state $\tilde{X}\ ^2B_2$ potential energy surface, the computed barrier is certainly too high given the available photon energy of roughly 4.4 eV. On the excited-state potential, the barrier is lower but also seems too high for dissociation to take place to CN + H_2. However, the barrier looks rather narrow and therefore, considering that the light H atom is involved, tunneling may play a role. On the other hand, tunneling should be rather slow and may only play a role in the absence of more efficient reaction channels.

4.2.4. $H_2CN \rightarrow CN + 2H$. Finally, Figure 8 shows the linear dissociation of both hydrogen atoms (reaction 2) at the MRCI level of theory, the angles and the C−N distance being kept fixed. As expected from Table 2, the ground state has a very deep Morse-like potential with a well depth of 7.14 eV. The higher lying $^2B_1$ state has a very deep Morse-like potential as well, whereas the lower lying $^2B_1$ state has a small barrier and becomes degenerate with the second $^2B_2$ state. The bright excited state shows no barrier and becomes degenerate with the ground state at the asymptote, 2.78 eV above its equilibrium energy. This is well above the asymptote for reaction 1 and rules out this reaction channel at the available photon energy of about 4.4 eV.

4.2.5. 2D Potential Energy Surface. To estimate the reaction barriers of reaction 3, we tried to optimize the transition state, which turned out to be very difficult as the system dissociated toward reaction 2. To gain further insight into reactions 2 and 3, we instead decided to compute a 2D potential energy surface of the bright excited state. To this end, the C−N distance has been kept fixed at a distance of 1.1840 Å, and the system was restricted to C_{2v} symmetry. This leaves two degrees of freedom, the H−H distance (denoted R_{H-H}) and the distance between the H−H and C−N fragments (R_{frg}). Figure 9 shows a contour plot along those coordinates. The equilibrium geometry is located at an interfragment distance of around 0.6 Å and R_{H-H} of around 2.0 Å. Reaction 3 proceeds toward a smaller H−H distance and larger interfragment distances; its transition state is roughly at 1.4 Å for the H−H distance and 1 Å for the interfragment distance. Once the barrier is passed, the potential descends steeply toward the fragments in the direction of the bottom-right corner of the plot.

The cut in Figure 8 (of reaction 2) represents the path from the equilibrium geometry toward larger H−H and interfragment distances (the upper-right corner of the plot). For large H−H distances, the potential energy surface becomes relatively flat.

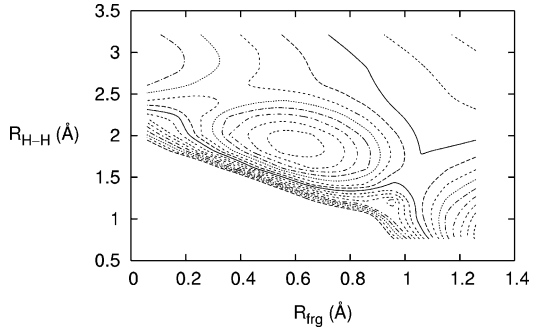

Figure 9. Contour plot of the 2D PES of H_2CN hydrogen displacements in C_{2v} symmetry. Contour lines are 0.2 eV apart. Hydrogen displacements are given in Å.

A small gradient toward smaller interfragment distances can be observed, however, resulting in a minimum at the top-left corner. Correspondingly, a second saddle point is observed at 2.5 Å for R_{H-H} and 0.35 Å for R_{frg}. This saddle point is about 0.25 eV lower in energy than the one for reaction 3, while the minimum is less pronounced. This shallow minimum corresponds to a weakly bound complex of two H atoms, interacting with the π orbitals of the CN radical. Comparing the potential energy surface with the excitation energies in our experiment, one can conclude that the energetically accessible region is confined to the equilibrium minimum, and the system is unlikely to dissociate through any of these channels. Of course, for higher excitation energies than available in the discussed experiments, such channels may become accessible.

5. Discussion

Prior to the recent theoretical study by Eisfeld,[16] the consensus was that the observed electronic transition in H_2CN was due to a dipole-forbidden but vibronically-allowed transition to the $\tilde{A}\ ^2B_1$ state. The experimental evidence for this assignment comes from the H atom photofragment study of Davis and co-workers.[7] They measured the angular distribution of the H atom photofragments by integrating Rydberg H-atom TOF spectra obtained at various polarization angles of the excitation laser. They determined a value of $\beta = -0.10 \pm 0.03$ for the recoil anisotropy parameter.[19] Careful checks were made to ensure that experimental artifacts did not contribute to the angular variation of the signal. The derived value of the recoil anisotropy parameter was interpreted in terms of the model for direct dissociation,[19] in which β equals $2P_2(\cos\theta_m)$, where θ_m is the angle between the recoil direction of the H atom (assumed to be along a C−H bond) and the direction of the E field of the excitation laser. Since the angle between the b inertial axis and a C−H bond is ∼30°, the recoil anisotropy parameter β should be positive for the $\tilde{B}\ ^2A_1 \leftarrow \tilde{X}\ ^2B_2$ transition according to this reasoning [$2P_2(\cos 30°) = +1.25$]. Hence, the slightly negative value for β measured by Davis and co-workers[7] would appear to rule out the $\tilde{B}\ ^2A_1 \leftarrow \tilde{X}\ ^2B_2$ assignment for the observed electronic transition in H_2CN.

There are several possible explanations for the observation by Davis and co-workers[7] of a negative recoil anisotropy parameter for the H atom fragments, which would not negate the $\tilde{B}\ ^2A_1 \leftarrow \tilde{X}\ ^2B_2$ assignment. In our CRD absorption spectra (Figure 3, parts b and c), the H_2CN bands are observed on an essentially zero background. By contrast, the H_2CN bands appear in the H atom photofragment action spectrum of Davis and co-workers[7] (Figure 3d) on a background which increases with decreasing wavelength. As discussed in section 4.1, it is likely that this background is due to photodissociation of residual formaldazine molecules in the molecular beam.

Felder et al.[30] investigated the 193 nm photodissociation of formaldazine by molecular-beam photofragment translational spectroscopy. The primary photodissociation channel leads to the formation of two H_2CN fragments, but it was found that approximately 80% of the H_2CN radicals possess enough energy to undergo secondary dissociation to H + HCN. The excited-state dissociation was rapid, and the recoil anisotropy parameter β was determined to equal $+0.90 \pm 0.05$, consistent with the assignment of the transition as $\pi^* \leftarrow \pi$, which has an in-plane transition moment. Formaldazine also has a weak electronic transition near 275 nm, which has been assigned[2] as a $\pi^* \leftarrow n$ transition; this assignment is consistent with a negative value for β. It is possible that the internally hot residual formaldazine in the molecular beam could fragment to produce H atoms upon irradiation at ∼285 nm.

As an alternative explanation of the negative value of β observed by Davis and co-workers,[7] it is likely that the model of direct dissociation does not apply to the $H_2CN\ \tilde{B}\ ^2A_1$ excited state. From the Lorentzian width parameters Γ derived from comparison of experimental and simulated spectra (see Figures 4 and 5), we estimate[31] that the excited-state dissociation lifetimes are 0.4 and 0.2 ps for the ground and $2\nu_4$ levels of the $\tilde{B}\ ^2A_1$ state. The A rotational constant for H_2CN is approximately 9 cm^{-1}. This implies that the period of rotation about the a inertial axis is ∼0.05 ps on average at room temperature. Thus, this suggests that dissociation does not occur on a time scale short compared to the rotational period, which is one of the assumptions of the direct dissociation model.

Dixon and Hancock[32] have derived expressions for the recoil anisotropy parameter β for the finite-lifetime predissociation of a symmetric top molecule and showed how these could be extended to asymmetric top molecules. This analysis shows that the value of β will depend on the precise irradiated wavelength within the rotational profile[33] of a band. Moreover, values of β inconsistent with the direct dissociation model can be observed. A particularly dramatic example of this is the observation by Kable et al.[33] of a parallel fragment distribution from excitation of a perpendicular transition in the HCO radical.

In fact, the theoretical study of the dissociation channels clearly shows that direct dissociation on the excited-state surface is not possible at the experimental photon energies. Thus, internal conversion is necessary prior to dissociation. Several conical intersections among excited states are found in calculations of the potential surfaces along symmetry coordinates (not shown here), but no intersection with the electronic ground state was observed in the energetically accessible region. Thus, the nonradiative decay to the electronic ground state is likely to be a fairly slow process.

Davis and co-workers[7] observed a broad kinetic energy distribution of H atom fragments from H_2CN photodissociation upon excitation of the origin band at 285 nm. From energy conservation, this corresponds to a broad range of vibrational energy, peaking at ∼16000 cm^{-1} in the HCN cofragment. Internal conversion of the $\tilde{B}\ ^2A_1$ excited state leads to the ground electronic state with total vibrational energy equal to the photon energy. This energy is much greater than the H−HCN dissociation energy, and the highly energized molecule will undergo unimolecular dissociation. Since there is no barrier to the dissociation process $H_2CN(\tilde{X}\ ^2B_2) \rightarrow HCN(\tilde{X}\ ^1\Sigma^+) + H(^2S)$ (see Figure 6), the available energy will be distributed statistically among the translational and HCN internal degrees of freedom. The HCN internal energy distribution, which can be obtained from the H atom time-of-flight spectrum measured by

Davis and co-workers,[7] is consistent with a statistical distribution of the available energy.

6. Conclusions

The absorption spectrum of the H_2CN radical, which was generated by 193 nm photolysis of formaldoxime, has been recorded by cavity ring-down spectroscopy. Two diffuse features were observed in the spectral range 34800−35800 cm^{-1}, along with the A−X (1,0) band of the OH photolytic cofragment. These features have been assigned as vibronic transitions of H_2CN. The rotational band shapes of the two bands were simulated based on the assumption of a B-type electronic transition, consistent with the $\tilde{B}\ ^2A_1 \leftarrow \tilde{X}\ ^2B_2$ assignment. The rotational constants were obtained from the ab initio geometries and appropriate expectation values of the moments of inertia tensor over the vibrational wave function of the corresponding state. Both bands are simulated in excellent agreement with experiment, giving strong evidence that the given assignment is correct. By contrast, the assumption of a transition to the $\tilde{A}\ ^2B_1$ state cannot be brought into agreement with the rotational profile of either of the bands. One significant point of disagreement between theory and experiment remains, namely the relative intensities of the two observed bands.

Insight has also been gained about the photodissociation mechanism. Extended high-level ab initio calculations show that at photon energies corresponding to 285 and 281 nm, respectively, all direct dissociation channels on the excited-state surfaces are inaccessible. Thus, internal conversion to the electronic ground state has to take place prior to dissociation. The computed dissociation energy of 30.3 kcal/mol is in excellent agreement with experimentally obtained values.[21] Thus, after excitation at 285 nm, an excess energy of 70.0 kcal/mol is available to the photofragments, which is very close to the maximum translational kinetic energy found for the H atoms in the experiment by Davis and co-workers.

The indirect photodissociation mechanism may also explain the discrepancy of the assigned electronic transition with the anisotropic recoil parameter measured by Davis and co-workers.[7] An excited-state lifetime of up to 0.4 ps is estimated from the rotational line widths obtained from the simulations. This is consistent with the internal conversion mechanism of dissociation and is an order of magnitude longer than the average rotational period of the radical. It therefore appears that the recoil anisotropy parameter cannot be used to determine the type of electronic transition in the present case, and thus there is indeed no conflict between the measurement and our assignment. We thus conclude that, based on our combined theoretical and experimental work, the observed absorption spectrum of H_2CN is due to the $\tilde{B}\ ^2A_1 \leftarrow \tilde{X}\ ^2B_2$ electronic transition.

Acknowledgment. We are extremely grateful to Floyd Davis for extensive illuminating and helpful correspondence about the details of the experiments described in ref 7. We also appreciate his sending data used in preparing Figure 3. The work at Johns Hopkins University was supported by the U.S. Army Research Office, under Grant No. DAAD19-02-1-0323. M.B. and W.E. are grateful for generous financial support by the Deutsche Forschungsgemeinschaft. We thank the Leibniz Rechenzentrum for the allocation of large amounts of computing time.

References and Notes

(1) Marston, G.; Steif, L. J. *Res. Chem. Intermed.* **1989**, *12*, 161.
(2) Ogilvie, J. F.; Horne, D. G. *J. Chem. Phys.* **1968**, *48*, 2248.
(3) Horne, D. G.; Norrish, R. G. W. *Proc. R. Soc. London, Ser. A* **1970**, *315*, 301.
(4) Horne, D. G.; Norrish, R. G. W. *Proc. R. Soc. London, Ser. A* **1970**, *315*, 287.
(5) Jacox, M. E. *J. Phys. Chem.* **1987**, *91*, 6595.
(6) Dagdigian, P. J.; Anderson, W. R.; Sausa, R. C.; Miziolek, A. W. *J. Phys. Chem.* **1989**, *93*, 6059.
(7) Bernard, E. J.; Strazisar, B. R.; Davis, H. F. *Chem. Phys. Lett.* **1999**, *313*, 461.
(8) Nizamov, B.; Dagdigian, P. J. *J. Phys. Chem. A* **2003**, *107*, 2256.
(9) Yamamoto, S.; Saito, S. *J. Chem. Phys.* **1992**, *96*, 4157.
(10) So, S. P. *Chem. Phys. Lett.* **1981**, *82*, 370.
(11) Adams, G. F.; Yarkony, D. R.; Bartlett, R. J.; Purvis, G. D. *Int. J. Quantum Chem.* **1983**, *23*, 437.
(12) Feller, D.; Davidson, E. R. *J. Chem. Phys.* **1984**, *80*, 1006.
(13) Bair, R. A.; Dunning, T. H. *J. Chem. Phys.* **1985**, *82*, 2280.
(14) Chipman, D. M.; Carmichael, L.; Feller, D. *J. Phys. Chem.* **1991**, *95*, 4702.
(15) Brinkmann, N. R.; Wesolowski, S. S.; Schaefer, H. F. *J. Chem. Phys.* **2001**, *114*, 3055.
(16) Eisfeld, W. *J. Chem. Phys.* **2004**, *120*, 6056.
(17) Eisfeld, W. *Phys. Chem. Chem. Phys.* **2005**, *7*, 832.
(18) Barone, V.; Carbonniere, P.; Pouchan, C. *J. Chem. Phys.* **2005**, *122*, 224308.
(19) Zare, R. N. *Angular Momentum*; Wiley-Interscence: New York, 1988.
(20) Herzberg, G. *Molecular Spectra and Molecular Structure III. Electronic Spectra and Electronic Structure of Polyatomic Molecules*; D. Van Nostrand: Princeton, NJ, 1967.
(21) Cowles, D. C.; Travers, M. J.; Frueh, J. L.; Ellision, G. B. *J. Chem. Phys.* **1991**, *94*, 3517; **1991**, *95*, 3864.
(22) Scholl, R. *Berichte* **1891**, *24*, 573.
(23) Werner, H.-J.; Knowles, P. J. *J. Chem. Phys.* **1988**, *89*, 5803.
(24) Knowles, P.-J.; Werner, H.-J. *Chem. Phys. Lett.* **1988**, *145*, 514.
(25) Davidson, E. R. *J. Comput. Phys.* **1975**, *17*, 87.
(26) Dunning, T. H. *J. Chem. Phys.* **1989**, *90*, 1007.
(27) Kendall, R. A.; Dunning, T. H. *J. Chem. Phys.* **1992**, *96*, 6796.
(28) Werner, H.-J.; Knowles, P. J.; Lindh, R.; Schütz, M.; Celani, P.; Korona, T.; Manby, F. R.; Rauhut, G.; Amos, R. D.; Bernhardsson, A.; Berning, A.; Cooper, D. L.; Deegan, M. J. O.; Dobbyn, A. J.; Eckert, F.; Hampel, C.; Hetzer, G.; Lloyd, A. W.; McNicholas, S. J.; Meyer, W.; Mura, M. E.; Nicklass, A.; Palmieri, P.; Pitzer, R.; Schumann, U.; Stoll, H.; Stone, A. J.; Tarroni, R.; Thorsteinsson, T. *MOLPRO, a package of ab initio programs designed by H.-J. Werner and P. J. Knowles*, version 2002.1; Cardiff University: U.K., 2002.
(29) Davis, H. F. Private communication, 2005.
(30) Felder, P.; Harrison, J. A.; Huber, J. R. *J. Phys. Chem.* **1991**, *95*, 1945.
(31) Lefebvre-Brion, H.; Field, R. W. *The Spectra and Dynamics of Diatomic Molecules*; Elsevier: Amsterdam, The Netherlands, 2004.
(32) Dixon, R. N.; Hancock, T. W. T. *J. Phys. Chem. A* **1997**, *101*, 7567.
(33) Kable, S. H.; Loison, J.-C.; Neyer, D. W.; Houston, P. L.; Burak, I.; Dixon, R. N. *J. Phys. Chem.* **1991**, *95*, 8013.